Precambrian Research 235 (2013) 251–263

Contents lists available at SciVerse ScienceDirect

Precambrian Research

journal homepage: www.elsevier.com/locate/precamres

The generation and evolution of Archean continental crust in the Dunhuang block, northeastern Tarim craton, northwestern China

Keqing Zong[a,*], Yongsheng Liu[a], Zeming Zhang[b], Zhenyu He[b], Zhaochu Hu[a], Jingliang Guo[a], Kang Chen[a]

[a] State Key Laboratory of Geological Processes and Mineral Resources, China University of Geosciences, Wuhan 430074, China
[b] Institute of Geology, Chinese Academy of Geological Sciences, No. 26, Baiwanzhuang Road, Beijing 100037, China

ARTICLE INFO

Article history:
Received 3 March 2013
Received in revised form 29 June 2013
Accepted 2 July 2013
Available online xxx

Keywords:
TTG
Archean
Continental crust
Crustal growth
Dunhuang block
Tarim craton

ABSTRACT

Tonalite–trondhjemite–granodiorite (TTG) preserved in Archean cratons can provide insights into the generation and evolution of the early continental crust. In this study, typical TTG gneisses from the Dunhuang block in the northeastern Tarim craton were studied in detail regarding their geochemistry and geochronology to constrain the generation and evolution of the Archean continental crust in this region. These TTG gneisses are characterized by high contents of SiO_2 (68.3–71.6%), Al_2O_3 (15.3–16.9%), Na_2O (4.43–4.85%), low K_2O/Na_2O ratios (0.20–0.37) and a very low HREE content (Yb < 1 ppm) and show two-stage Nd isotope model ages of ~3.06–2.84 Ga. Zircon U–Pb analyses reveal that these TTG gneisses were formed ~2.7–2.6 Ga ago, as shown by inherited magmatic zircon cores, and were later altered by Paleoproterozoic (~2.0–1.9 Ga) and early Paleozoic (~430 Ma) high-grade metamorphic events. Two samples show positive $\varepsilon_{Hf}(t)$ values of 1.5–5.4 for magmatic zircons with ages of ~2.7–2.6 Ga and give a two-stage Hf isotope model age of ~2.95 Ga, while one sample exhibits negative $\varepsilon_{Hf}(t)$ values of −3.4 to −7.2 for magmatic zircons with ages of ~2.7–2.6 Ga and gives a two-stage Hf isotope model age of ~3.4 Ga, suggesting that the Paleoarchean and Mesoarchean Eras were important periods for the generation of juvenile continental crust in the Dunhuang block. Lastly, based on analyses of previous studies, we speculate that the Tarim craton has been subjected to episodic crustal growths at ~3.4 Ga, ~3.2 Ga, ~2.95 Ga, ~2.8 Ga and ~2.6 Ga and reworking events at ~2.7–2.6 Ga and ~2.5 Ga

1. Introduction

The continental crust is the archive of the geological history of the Earth (Cawood et al., 2013; Condie and Kröner, 2013; Hawkesworth et al., 2010; Roberts, 2012). Understanding the generation and evolution of the continental crust plays a key role in the earth sciences because changes in the volume of the continental crust and the distribution of continents on Earth's surface have profound effects on many geological processes through Earth's history (Condie, 2005; Hawkesworth et al., 2010). It is widely accepted the majority of the continental crust (>70%) most likely formed in the Archean (Cawood et al., 2013; Taylor and McLennan, 1995). Sodium-rich tonalite–trondhjemite–granodiorite (TTG) suites are generally considered to be one of the most important lithologies of Archean rocks, which constitute more than 80% of the surviving Archean continental crust (Martin et al., 2005; Moyen and Martin, 2012). Therefore, TTG gneisses preserved in various Archean cratons can be used to decipher the generation and evolution of the early continental crust.

The North China, South China and Tarim cratons are the three largest cratons in China and are separated from and sutured to each other by Phanerozoic orogenic belts and faults (insert figure in Fig. 1). Compared to the extensively studied North China and South China cratons, the Tarim craton is poorly understood (Zhao and Cawood, 2012; Zheng et al., 2013 and within references). This is largely because more than 85% of the Tarim craton is covered by desert and gobi, and as a result the Precambrian basement rocks are only locally exposed on the margins of this craton (Lu et al., 2008; Zhang et al., 2012b; Zhao and Guo, 2012). The Archean TTG gneisses are primarily exposed in the Kuluketage and Dunhuang blocks on the northern and northeastern margins of the Tarim craton, respectively (Fig. 1). The Neoarchean TTG gneisses within the Kuluketage area have been studied recently (Long et al., 2010, 2011; Lu et al., 2008; Zhang et al., 2012a). Those results revealed that these TTG gneisses mainly formed ~2.65–2.5 Ga ago (Long et al., 2010, 2011; Lu et al., 2008; Zhang et al., 2012a) and were overprinted by Paleoproterozoic (~1.9–1.8 Ga) tectonothermal events (Zhang et al., 2012a). However, detailed geochemical and

* Corresponding author. Tel.: +86 15994222021; fax: +86-27-67885096.
E-mail address: kqzong@hotmail.com (K. Zong).

0301-9268/$ – see front matter © 2013 Elsevier B.V. All rights reserved.
http://dx.doi.org/10.1016/j.precamres.2013.07.002

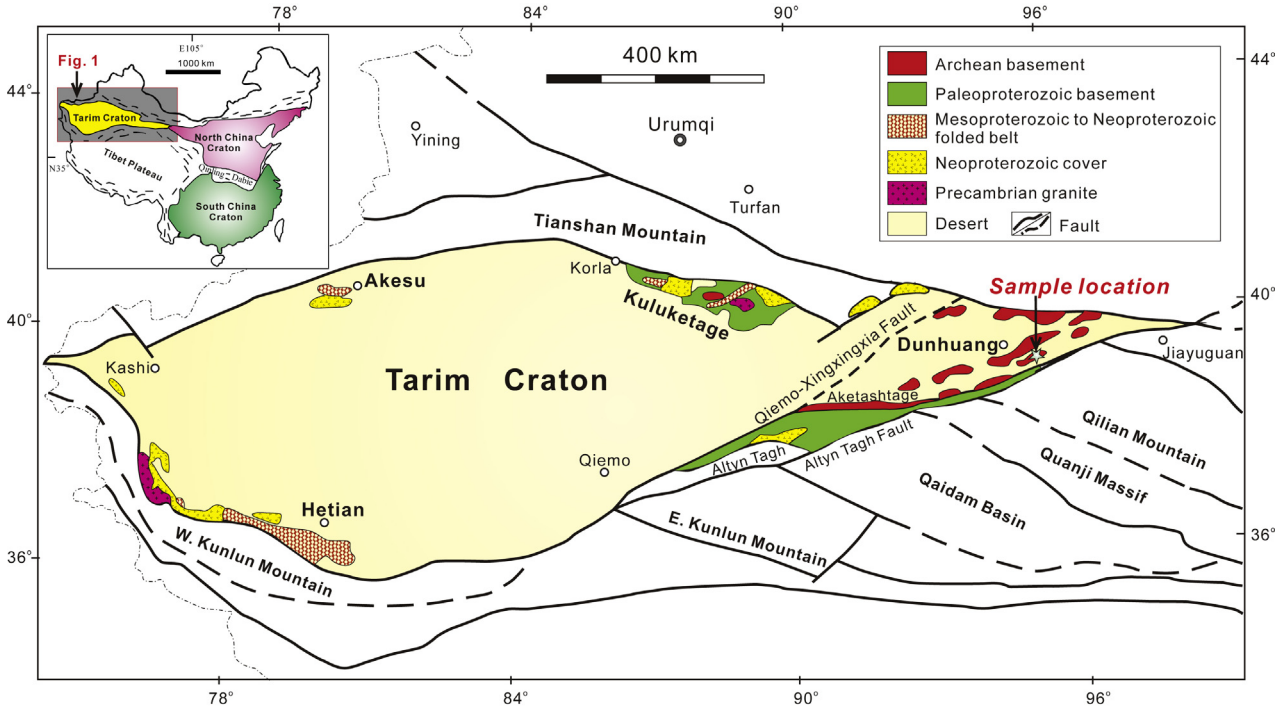

Fig. 1. Simplified geological map of the Tarim craton and adjacent areas (modified after Lu et al., 2008; Zhao and Cawood, 2012). Insert figure shows a simplified tectonic map of China.

geochronological information from the Archean TTG in the Dunhuang block, in which significant amounts of the Archean rocks in the Tarim craton are exposed (Fig. 1), is scarce. On the basis of thermal ionization mass spectrometer (TIMS) U–Pb zircon dating of one tonalite, Mei et al. (1998) suggested that TTG in the Dunhuang block formed in 2.67 Ga and underwent Neoproterozoic (~1.0 Ga) alteration. Recently, Zhang et al. (2013b) proposed that TTG gneiss in the Dunhuang block underwent a ~2.5 Ga magmatic–metamorphic event. In contrast, episodes of Paleoproterozoic (~1.85 Ga) and early Paleozoic (~430 Ma) high-pressure granulite metamorphism have been well described in the Dunhuang block by Zhang et al. (2012c) and Zong et al. (2012), respectively, and these findings indicate that the Neoarchean-generated TTG in the Dunhuang block most likely experienced a prolonged and complex continental crust evolution. Thus, more detailed work on Archean TTG gneiss in the Dunhuang block especially regarding its in situ geochronology is needed to refine the constraints on the generation and evolution of the early continental crust in the Tarim craton.

In this paper, we summarize our petrological investigation and analyses of element and Sr–Nd isotope compositions of whole-rock and in situ zircon U–Pb dating and Hf isotope compositions of three typical TTG gneisses from the Dunhuang block. In situ zircon U–Pb results showed that these TTG gneisses formed ~2.7–2.6 Ga ago and were overprinted by Paleoproterozoic (~2.0–1.9 Ga old) and Paleozoic (~430 Ma old) tectonothermal events. When combining our findings with previous studies, we found that the Hf isotope compositions of zircons revealed the episodic continental crustal growth during the Paleoarchean to Neoarchean Eras and that Paleoarchean continental crust as old as ~3.4 Ga may have existed in the Dunhuang block.

2. Geological background and samples

The Tarim craton, located in the northwestern China, is one of three major Precambrian cratonic blocks in China and covers an area of more than 600,000 km^2. This craton has the physiographic appearance of a large eyeball when viewed from high altitude and is bounded by the Tianshan Mountains on the north, the western Kunlun Mountains on the south, and the Altyn Tagh on the southeast (Fig. 1). Its central part is covered by Cenozoic desert, and the Precambrian basement rocks are only distributed along the margins of the Tarim Basin, including Akesu area in the northwestern margin, Hetian area in the southwestern margin, the Kuluketage area in the northern margin, the North Altyn Tagh and the Dunhuang area in the northeastern margin (Fig. 1). The Aksu group in Aksu area have suffered from blueschist-facies metamorphism with disputed Neoproterozoic metamorphic ages of ~872–700 Ma (Chen et al., 2004; Liou et al., 1996; Nakajima et al., 1990; Yong et al., 2013). The oldest rock in the Hetian area is Akazi granodiorite with formation age of ~2.41 Ga and metamorphic age at ~1.9 Ga (Zhang et al., 2012b). The Neoarchean (~2.65–2.5) rocks in the Kuluketage area are mainly consisted of TTG gneiss with amphibolite enclaves, calc-alkaline granites and high Ba–Sr granites, which underwent metamorphic event at ~1.9–1.8 Ga (Long et al., 2010, 2011; Zhang et al., 2012a). The North Altyn Tagh–Dunhuang area in the northeastern margin of Tarim craton is traditionally called the Dunhuang block, which is a triangular block bounded on the north by Beishan Mountain, on the northwest by the Qiemo-Xingxingxia fault and on the southeast by the Altyn Tagh fault (Fig. 1). The Dunhuang block is composed of a series of supracrustal rocks that underwent medium- to high-grade metamorphism, called the "Dunhuang Group", and subordinate volumes of TTG intrusions (Mei et al., 1997). The Dunhuang Group is dominated by metasedimentary rocks, including garnet-kyanite schist, graphite-bearing marble, garnet amphibolite, gneiss and quartzite, and a few metavolcanic rocks and has some features of "khondalite series" (Mei et al., 1997; Yu et al., 1998). Although Archean TTG gneiss was emphasized as an important lithology in the Dunhuang block (Mei et al., 1997; Yu et al., 1998), the limited geochronological work only focused on the southern margin of the Dunhuang block (Mei et al., 1998; Zhang et al., 2013b). These Archean rocks include the tonalitic gneiss at the Shibaocheng area with a TIMS U–Pb zircon age of 2670 ± 12 Ma (Mei et al., 1998),

the tonalitic gneiss from the Aketashitage area with SHRIMP U–Pb zircon ages of 2567 ± 32 Ma (Liu et al., 2009b). Recently, Zhang et al. (2012c; 2013b) reported a ~2.5 Ga magmatic–metamorphic event and a ~1.85 Ga HP granulite facies metamorphism from the Hongliuhe–Shibaocheng area.

In our study, three representative TTG gneisses (X11-113-2, X11-114-1 and X11-122-1) near the town of Dongbatu in the interior of the Dunhuang block were selected for element and Sr–Nd isotope analysis of whole-rock and in situ zircon U–Pb dating and trace-element and Hf isotope analysis. Because of the strong deformation and metamorphism, the detailed field relationship between these TTG gneisses and the host Dunhuang Group is unclear. In summary, the studied TTG gneisses always occur sporadically as blocks in the Dunhuang Group. These samples are gray, medium- to coarse-grained and show granoblastic textures with gneissic structures (Fig. 2). The rocks consist mainly of plagioclase (~58%), quartz (~30%), biotite (~10%) with accessory *K*-feldspar, epidote, titanite, apatite and zircon (Fig. 2). On the other hand, a few outcrops contain strong gneissic foliation with some garnet-rich felsic vein consisting mainly of garnet, biotite and plagioclase.

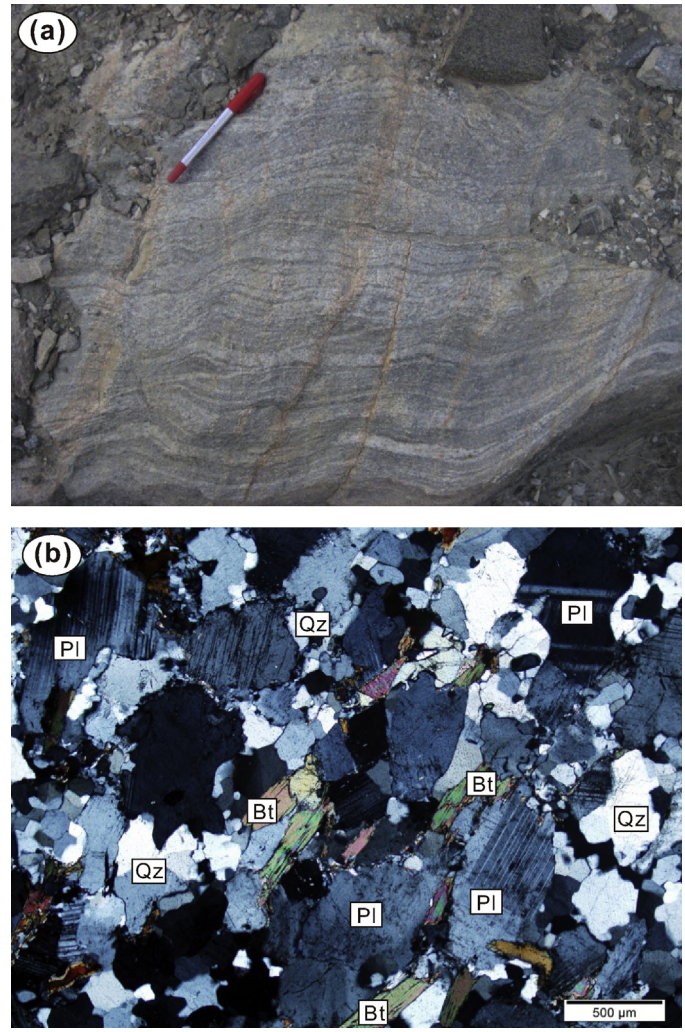

Fig. 2. Field exposures (a) and the main mineral assemblage (b) of TTG gneiss in the Dunhuang block. Pl = plagioclase, Qz = quartz, Bt = biotite.

3. Analytical methods

3.1. Elemental and Sr–Nd isotopic analysis of whole rock

Whole-rock samples were crushed in a corundum jaw crusher down to 60 mesh size. Approximately 50 g from each sample was powdered in an agate ring mill to less than 200 mesh size. The major elements were analyzed using X-ray fluorescence (Shimadzu XRF-1800) at the State Key Laboratory of Geological Processes and Mineral Resources, China University of Geosciences, Wuhan. The analytical precision and accuracy for major elements were better than 4%. These sample preparation and analytical procedures have been described in detail by Ma et al. (2012). Trace elements were analyzed using an Agilent 7500a ICP–MS at the State Key Laboratory of Geological Processes and Mineral Resources, China University of Geosciences, Wuhan. Samples measuring approximately 50 mg were digested by HF + HNO_3 in Teflon bombs for ICP–MS analysis. The sample-digesting procedure for ICP–MS analyses and the analytical precision and accuracy for trace elements were the same as those described by Liu et al. (2008b).

Sr-Nd isotopic ratios were analyzed on a Triton TI mass spectrometer (Thermo Finnigan, Germany) operated in static mode at the State Key Laboratory of Geological Processes and Mineral Resources, China University of Geosciences, Wuhan. Full details of the Rb–Sr and Sm–Nd procedures were reported in Gao et al. (2004). $^{87}Rb/^{86}Sr$ and $^{147}Sm/^{144}Nd$ ratios were calculated from measured whole rock Rb, Sr, Sm and Nd contents determined by ICP–MS.

3.2. Zircon U–Pb dating and trace element analysis by LA–ICP–MS

Zircon grains were separated by a conventional mineral-separation technique, mounted in epoxy resin, polished and then cleaned in a 5% HNO_3 bath with an ultrasonic washer prior to analysis. The U–Pb dating and trace-element analysis of zircons were performed simultaneously by LA–ICP–MS at the State Key Laboratory of Geological Processes and Mineral Resources, China University of Geosciences, Wuhan. The operating conditions for the laser ablation system and the ICP–MS instrument were the same as those described by Liu et al. (2010a, 2008a, 2010b). Laser sampling was conducted using a GeoLas 2005 System with a spot size of 32 μm. An Agilent 7500a ICP–MS instrument was used to acquire ion-signal intensities. To keep time-dependent elemental fractionation at a low level, a laser frequency of 4 Hz and laser energy of 60 mJ were applied (Zong et al., 2010). Zircon standard 91,500 was used as an external standard to calibrate isotope fractionation, which was analyzed twice for every 5 analyses. NIST 610 was analyzed every 10 analyses in order to correct the time-dependent drift of sensitivity and mass discrimination for the trace-element analysis. The trace-element compositions were calibrated against NIST 610, using Zr as an internal standard (Liu et al., 2008a). Off-line selection and integration of background and analytical signals and time-drift correction and quantitative calibration were conducted using ICPMSDataCal (Liu et al., 2008a, 2010a). The obtained concordia age (599 ± 2 Ma, n = 9) and $^{206}Pb/^{238}U$ age (598 ± 4 Ma, n = 9) of zircon standard GJ-1 agrees well with the preferred ID–TIMS $^{206}Pb/^{238}U$ age of 599.8 ± 4.8 Ma (2σ) (Jackson et al., 2004) within analytical uncertainty. Except for those elements with extremely low concentrations (e.g., La, Pr and Nd) close to the method detection limit of LA–ICP–MS, the results of trace element compositions of zircon standard 91,500 and GJ-1 are generally consistent with the LA–ICP–MS working values and solution-ICP–MS results within 10% relative deviations, respectively.

3.3. Zircon Hf isotope ratio analysis by LA–MC–ICP–MS

The experiments were conducted using a Neptune Plus MC–ICP–MS (Thermo Fisher Scientific, Germany) and a Geolas 2005 excimer ArF laser ablation system (Lambda Physik,

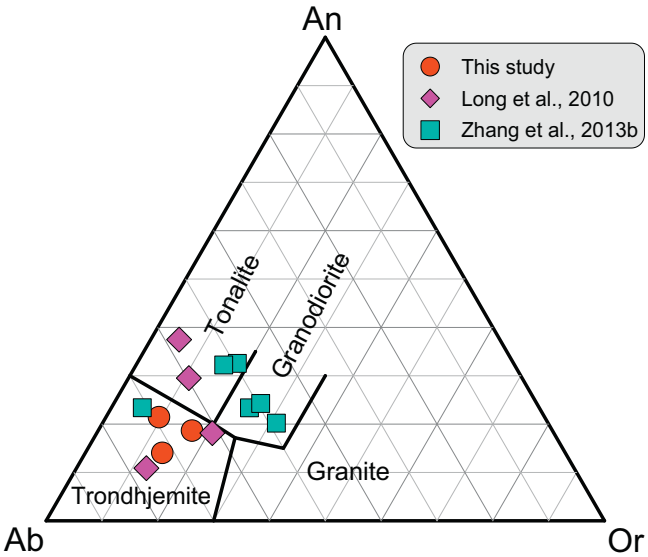

Fig. 3. Classification of TTG gneiss from the Tarim craton on the basis of normative anorthite (An), albite (Ab) and orthoclase (Or), as defined by Barker (1979).

Göttingen, Germany), which were available for our use at the State Key Laboratory of Geological Processes and Mineral Resources, China University of Geosciences, Wuhan. The energy density of laser ablation used in this study was 5.3 J cm^{-2}. Helium was used as the carrier gas in the ablation cell and was merged with argon (makeup gas) after the ablation cell. As demonstrated by our previous study, for the 193 nm laser a more consistent 2-fold signal enhancement was achieved in helium than in argon gas (Hu et al., 2008b). We used a simple Y junction downstream from the sample cell to add small amounts of nitrogen (at a rate of 4 ml min^{-1}) to the argon makeup gas flow (Hu et al., 2008a). Compared to the standard arrangement, the addition of nitrogen and our use of the newly designed X skimmer cone and Jet sample cone in the Neptune Plus improved the signal intensity of Hf, Yb and Lu by a factor of 5.3, 4.0 and 2.4, respectively. All data from zircon in this study were acquired in the single-spot ablation mode at a spot size of 32 μm. Each measurement consisted of 20 s of acquisition of the background signal followed by 50 s of ablation signal acquisition. The operating conditions for the laser ablation system and the MC–ICP–MS instrument and the analytical method are the same as those described in detail by Hu et al. (2012). Our off-line selection and integration of analyte signals and mass bias calibrations were performed using ICPMSDataCal (Liu et al., 2008a, 2010a). The obtained zircon Hf isotopic compositions of the standards were 0.282015 ± 0.000006 (2σ, n = 11) for GJ-1, 0.282694 ± 0.000007 (2σ, n = 14) for Temora-2 and 0.282299 ± 0.000006 (2σ, n = 32) for 91,500.

Table 1
Major and trace element compositions of TTG gneisses in the Dunhuang block, northeastern Tarim craton.

Sample	X11-113-2	X11-114-1	X11-122-1
Location	N: 40°07, 027″ E: 95°43, 413″	N: 40°07, 058″ E: 95°43, 412″	N: 40°06, 789″ E: 95°43, 369″
Major element compositions (wt%)			
SiO_2	68.29	69.86	71.63
Al_2O_3	16.90	15.32	16.02
Fe_2O_3	2.71	3.44	2.17
CaO	3.28	3.01	3.44
MgO	1.40	1.39	0.98
K_2O	1.80	1.21	0.95
Na_2O	4.84	4.43	4.85
TiO_2	0.33	0.37	0.32
MnO	0.044	0.049	0.017
P_2O_5	0.019	0.059	0.103
LOI	0.72	1.19	0.62
CO_2	0.72	1.19	0.62
Total	100.3	100.3	101.1
K_2O/Na_2O	0.37	0.27	0.20
Trace element compositions (ppm)			
Li	17.2	16.7	9.62
Be	2.31	0.91	2.21
Sc	5.75	6.01	3.65
V	33.2	37.0	23.4
Cr	11.2	6.46	7.81
Co	6.16	7.22	5.46
Ni	8.36	6.30	11.1
Cu	9.06	18.1	4.23
Zn	35.4	43.4	31.4
Ga	19.2	18.8	21.2
Rb	52.6	40.6	35.5
Sr	445	458	574
Y	9.64	7.73	3.46
Zr	79.7	103	45.8
Nb	5.71	3.44	10.5
Cs	0.97	0.73	0.52
Ba	545	634	434
La	22.5	29.9	14.2
Ce	37.7	53.2	25.2
Pr	3.74	5.37	2.72
Nd	12.5	17.9	9.35
Sm	1.74	2.65	1.73
Eu	0.81	0.96	0.79
Gd	1.31	1.92	1.30
Tb	0.22	0.28	0.16
Dy	1.41	1.55	0.69
Ho	0.29	0.29	0.13
Er	0.89	0.82	0.30
Tm	0.13	0.10	0.034
Yb	0.81	0.59	0.15
Lu	0.10	0.08	0.02
Hf	2.07	2.74	1.18
Ta	0.20	0.12	0.29
Pb	11.6	16.5	13.4
Th	3.75	10.3	0.82
U	0.49	0.33	0.43

4. Results

4.1. Elemental and Sr–Nd isotopic compositions of the whole rocks

The major and trace-element compositions of the samples are shown in Table 1 and Figs. 3–5. These TTG gneisses show high percentages of SiO_2 (68.3–71.6%), Al_2O_3 (15.3–16.9%), and Na_2O (4.43–4.85%) and low K_2O/Na_2O ratios (0.20–0.37). They are poor in ferromagnesian elements (Fe_2O_3 + MgO + MnO + TiO_2 = 3.5–5.2%), with Mg# of 45–51 and Ni and Cr contents of 6.3–11.1 ppm and 6.5–11.2 ppm, respectively. According to the normative An–Ab–Or triangle classification for granitoids containing more than 10% normative quartz (Barker, 1979), these samples plot in the field of trondhjemite (Fig. 3). Concurrently, these samples are characterized by high LREE (La = 14.2–29.9) and low HREE contents (Yb = 0.15–0.81) (Table 1 and Fig. 4a), resulting in high La_N/Yb_N ratios ranging from 18 to 64 (Fig. 5), and exhibit slightly positive Eu and Sr anomalies and obviously negative Nb, Ta and Ti anomalies (Fig. 4a, b).

Sr–Nd isotopic compositions of these TTG gneisses are listed in Table 2. As we will be described below, sample X11-113-2, X11-114-1 and X11-122-1 have crystallization ages of 2717 Ma, 2642 Ma and 2708 Ma, respectively. Their $\varepsilon_{Nd}(t)$ values are 1.99, −1.26 and 0.72, respectively. Their T_{DM2} values vary from 3.06 to 2.84 Ga.

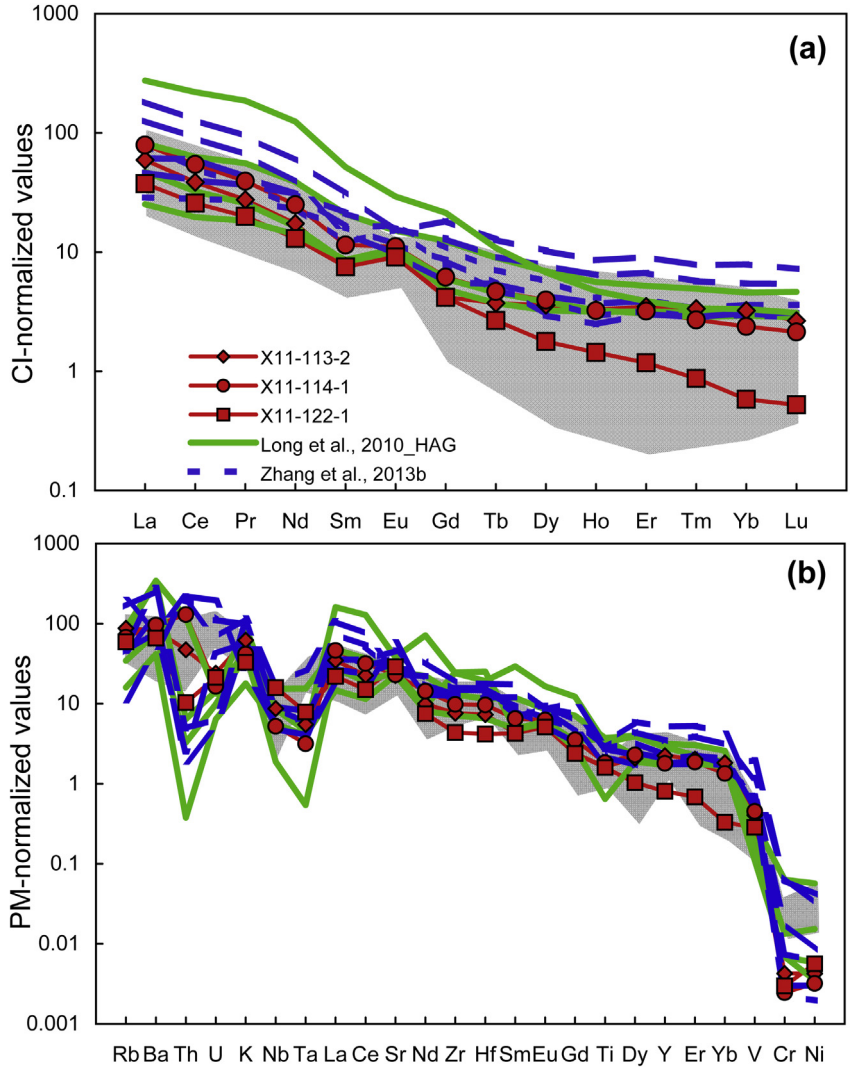

Fig. 4. CI-normalized REE pattern (a) and PM-normalized spider diagram (b) of TTG gneiss in the Tarim craton. Chondrite (CI) and primitive mantle (PM) values are from Masuda et al. (1973) and McDonough and Sun (1995), respectively. The shadow field represents the average trace element compositions of worldwide TTG gneiss with low and moderate HREE (Moyen and Martin, 2012).

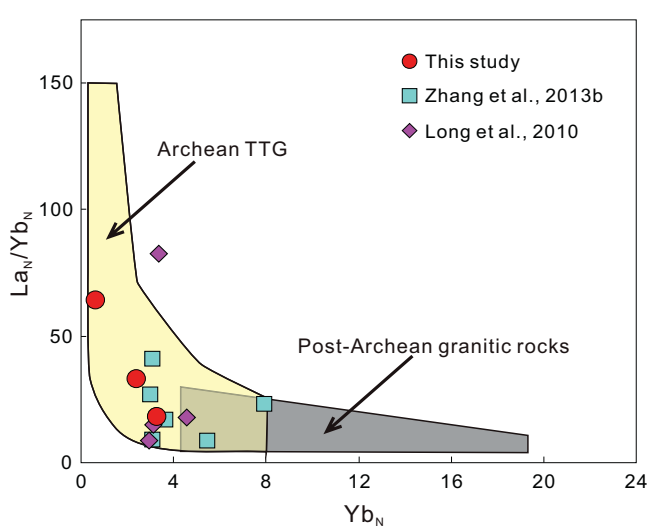

Fig. 5. $(La/Yb)_N$ versus Yb_N plot for TTG gneiss in the Tarim craton. The fields of Archean TTG and post-Archean granitic rocks are from Moyen and Martin (2012). Chondrite (CI) values are from Masuda et al. (1973).

Table 2
Sr-Nd isotopic compositions of TTG gneisses in the Dunhuang block, northeastern Tarim craton[a]

	X11-113-2	X11-114-1	X11-122-1
Rb (ppm)	52.6	40.6	35.5
Sr (ppm)	445	458	574
Sm (ppm)	1.74	2.65	1.73
Nd (ppm)	12.5	17.9	9.35
$^{87}Rb/^{86}Sr$	0.3418	0.2565	0.1789
$^{147}Sm/^{144}Nd$	0.0847	0.0892	0.1119
$^{87}Sr/^{86}Sr$	0.721253	0.720769	0.716436
2σ	0.000004	0.000004	0.000004
$^{143}Nd/^{144}Nd$	0.510594	0.510690	0.511235
2σ	0.000017	0.000008	0.000005
Crystallization age (Ma)	2717	2642	2708
$^{87}Sr/^{86}Sr$ (t)	0.707807	0.710965	0.709421
$^{143}Nd/^{144}Nd$ (t)	0.509076	0.509135	0.509236
T_{DM1} (Ga)	3.00	2.99	2.85
T_{DM2} (Ga)	3.06	3.06	2.84
$\varepsilon_{Nd}(0)$	−39.9	−38.0	−27.4
$\varepsilon_{Nd}(t)$	1.99	−1.26	0.72

[a] The decay constant (λ) of ^{147}Sm used in model age calculation is 0.00654 Ga^{-1}. $T_{DM1} = 1/\lambda \times \ln\{1 + [(^{143}Nd/^{144}Nd)sample - 0.51315]/[(^{147}Sm/^{144}Nd)sample - 0.2137]\}$. Two-stage Nd isotope model ages (T_{DM2}) were calculated relative to the average continental crust.

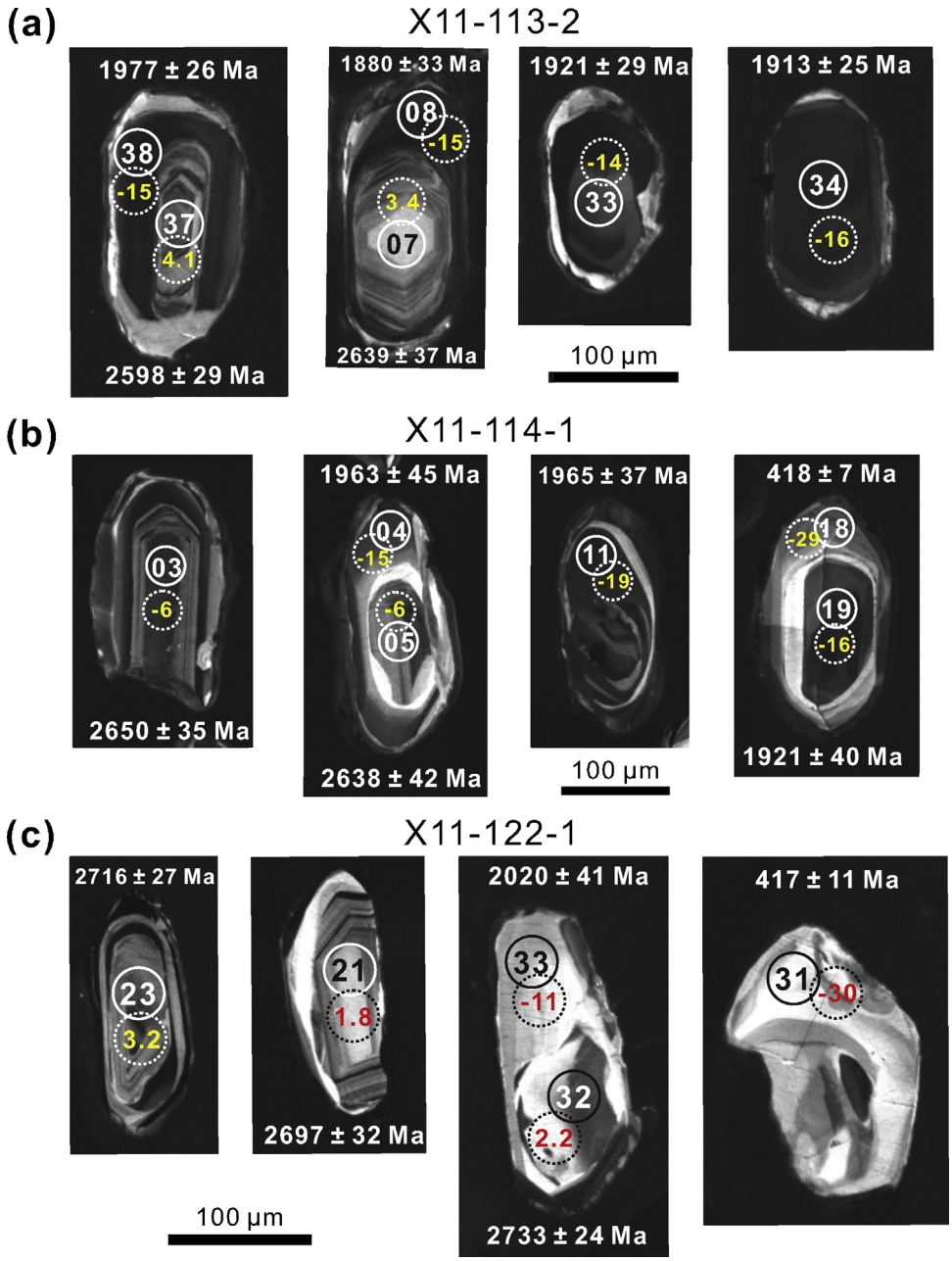

Fig. 6. Representative CL images of zircons in TTG gneiss from the Dunhuang block. The solid line circle and enclosed number represent the spot of LA–ICP–MS analysis for U–Pb dating and its analyzed number, respectively. The dashed-line circle and enclosed number represent the spot of LA–MC–ICP–MS analysis for Hf isotope and its $\varepsilon_{Hf}(t)$ value, respectively. Zircon U–Pb ages correspond to $^{206}Pb/^{238}U$ data with 1σ uncertainty.

4.2. Zircon U–Pb ages and trace element compositions

U–Pb ages and trace-element compositions of zircons analyzed by LA–ICP–MS are summarized in Supplementary Tables 1–3 and shown in Figs. 6 and 7. The euhedral and/or subhedral zircon grains separated from these samples show clear core-mantle-rim or core-rim structures in CL images (Fig. 6). Inherited cores in these zircon grains with core–mantle–rim structures uniformly exhibit oscillatory zoning in CL images (Fig. 6). Although most U–Pb ages of these inherited zircon cores are discordant (Supplementary Tables 1–3), because of Pb-loss induced by later tectonothermal events, they have relatively consistent $^{206}Pb/^{207}Pb$ ages that plot along a highly discordant line with upper-intercept ages of 2717 ± 31 Ma (2σ, n = 19, MSWD = 0.95), 2642 ± 63 Ma (2σ, n = 19, MSWD = 0.34) and 2708 ± 54 Ma (2σ, n = 19, MSWD = 3.8) for samples X11-113-2, X11-114-1 and X11-122-1 (Fig. 7a,c,e), respectively. Most of the homogenous dark/cloudy mantles (or cores in core-rim structures) also display discordant U–Pb ages (Supplementary Tables 1–3), but they are plotted on the discordant line in the U–Pb concordia diagram, with upper intercept ages of 1914 ± 45 Ma (2σ, n = 16, MSWD = 1.1), 2002 ± 31 Ma (2σ, n = 9, MSWD = 0.40) and 1966 ± 40 Ma (2σ, n = 14, MSWD = 5.1) for samples X11-113-2, X11-114-1 and X11-122-1 (Fig. 7a, c, e), respectively. Most of the bright zircon outermost rims are narrow, and only a few rims were analyzed using the applied spot size of 32 μm. Three analysis spots from sample X11-114-1 give a concordia U–Pb age of 417 ± 6 Ma (2σ, n = 3, MSWD = 0.06) (Fig. 7c) and a weighted $^{206}Pb/^{238}U$ age of 417 ± 12 Ma (2σ, n = 3). Two analysis spots from sample X11-122-1 have consistent $^{206}Pb/^{238}U$ ages and yield a weighted $^{206}Pb/^{238}U$ age of 428 ± 15 Ma (2σ, n = 2) (Fig. 7e).

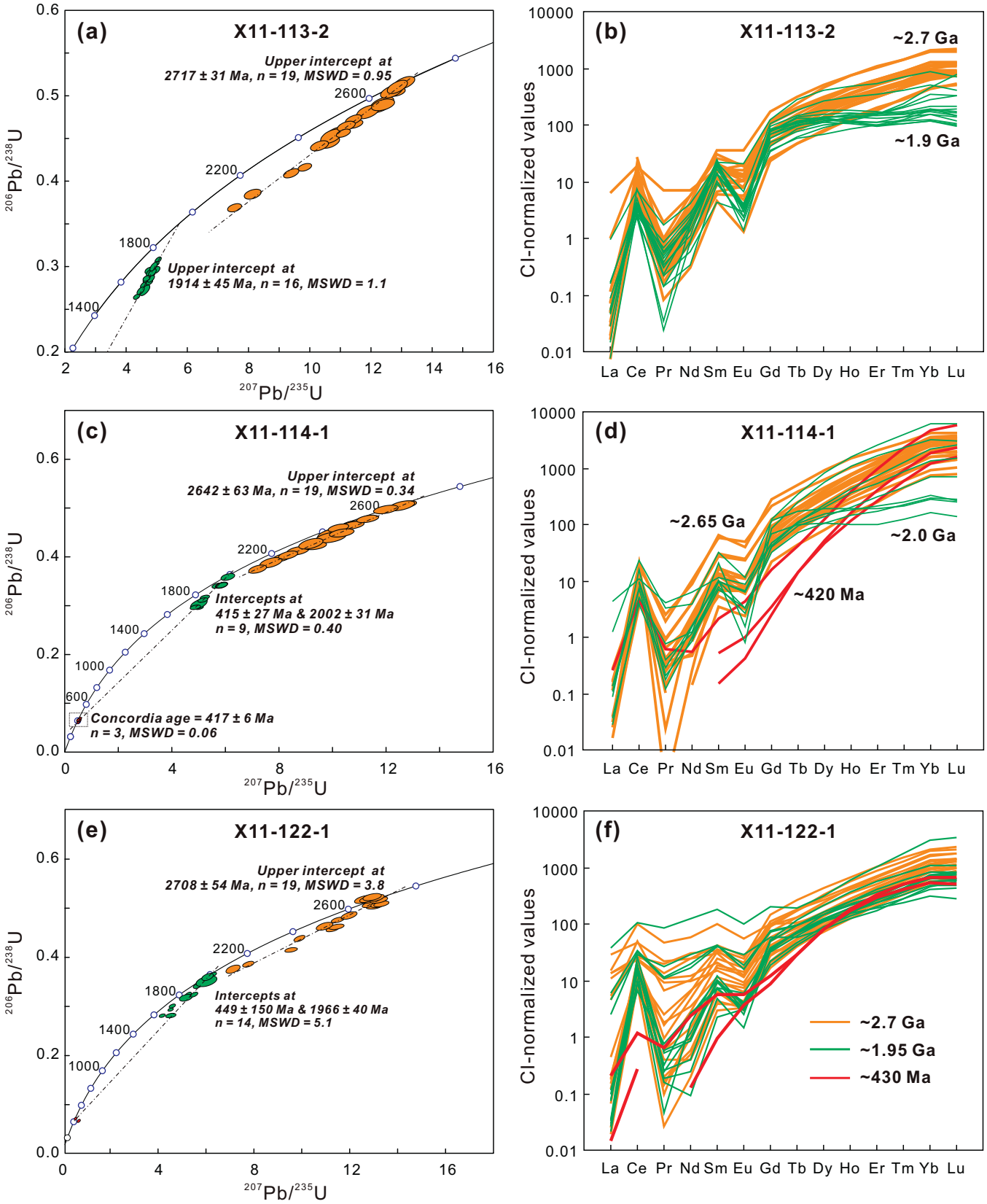

Fig. 7. Concordia diagrams (a, c, e) and CI-normalized REE patterns (b,d,f) of zircons in TTG gneiss from the Dunhuang block. Chondrite (CI) values from Masuda et al. (1973).

Supplementary data related to this article found, in the online version, at http://dx.doi.org/10.1016/j.precamres.2013.07.002.

The inherited zircon cores with ages of ~2.7–2.6 Ga in these samples show steep HREE patterns, positive Ce anomalies, negative Eu anomalies and high Th/U ratios (0.10–0.78) (Fig. 7b, d, f and Supplementary Tables 1–3). The zircon mantles/cores with ages of ~1.9 Ga in sample X11-113-2 exhibit flat HREE patterns, positive Ce anomalies,

negative Eu anomalies and low Th/U ratios (0.03–0.13) (Fig. 7b and Supplementary Table 1). However, the zircon mantles/cores with ages of ~1.95 Ga in sample X11–122–1 show steep HREE patterns, positive Ce anomalies, negative Eu anomalies and relatively high Th/U ratios (0.05–1.62) (Fig. 7f and Supplementary Table 3). While the zircon mantles/cores with ages of ~2.0 Ga in sample X11-114-1 have both flat and steep HREE patterns with positive Ce anomalies and negative Eu anomalies (Fig. 7d and Supplementary Table 2), the outermost rims of zircon with ages of ~430–420 Ma in samples X11-114-1 and X11-122-1 have relatively low LREE and MREE contents, very steep HREE patterns and low Th/U ratios (0.001–0.03) (Fig. 7d, f and Supplementary Tables 2–3).

4.3. Zircon Lu–Hf isotope compositions

The Lu–Hf isotope compositions of the analyzed zircons are summarized in Table 3 and shown in Fig. 8. The inherited zircon cores with ages of ~2.7–2.6 Ga in these TTG gneisses have low initial $^{176}Hf/^{177}Hf$ ratios, of 0.28113–0.28120, 0.28089–0.28100 and 0.28109–0.28115, as shown by analyses of samples X11-113-2, X11-114-1 and X11-122-1 (Table 3), respectively. The zircon mantles/cores with ages of ~2.0–1.9 Ga have initial $^{176}Hf/^{177}Hf$ ratios similar to those of inherited zircon cores with ages of ~2.7–2.6 Ga (Table 3). However, the outermost rims of zircon with ages of ~430–420 Ma exhibit obviously high initial $^{176}Hf/^{177}Hf$ ratios, of 0.28143–0.28170 and 0.28161–0.28179, as shown by analyses of samples X11-114-1 and X11-122-1 (Table 3), respectively. The zircon cores with ages of ~2.7–2.6 Ga in samples X11-113-2 and X11-122-1 are characterized by positive $\varepsilon_{Hf}(t)$ values of 3.1–5.4 and 1.5–3.6 and relatively young two-stage Hf isotope model ages (T_{DM2}) of ~2.9 Ga and ~3.0 Ga, respectively (Table 3 and Fig. 8). In contrast, zircon cores with ages of ~2.7 Ga in sample X11–114–1 show negative $\varepsilon_{Hf}(t)$ values of −3.4 to −7.2 and old T_{DM2} ages of 3.4–3.2 Ga (Table 3 and Fig. 8).

5. Discussion

5.1. Timing of Archean TTG gneiss in the Dunhuang block, northeastern Tarim craton

Zircon is an important tool in the absolute age dating of rocks and the basis for the geological time scale and can offer robust data for analyzing the record of magmatic and crust-forming events preserved in the continental crust (Corfu, 2013; Hawkesworth et al., 2010). In this study, TTG gneisses in the Dunhuang block show petrological (Fig. 2) and geochemical (Figs. 3–5) signatures consistent with typical TTG gneisses elsewhere in the world (Martin et al., 2005; Moyen and Martin, 2012). The inherited zircon cores in these samples show oscillatory zoning in CL images (Fig. 6), suggesting magmatic zircon precursors (Corfu et al., 2003). This is consistent with their steep HREE patterns, positive Ce anomalies, negative Eu anomalies and high Th/U ratios, which are commonly observed in magmatic zircons (Hoskin and Schaltegger, 2003; Rubatto, 2002). Thus, the upper intercept ages of 2717 ± 31 Ma (2σ, n = 19), 2642 ± 63 Ma (2σ, n = 19) and 2708 ± 54 Ma (2σ, n = 19) yielded by these inherited zircon cores represent the formational ages of these TTG gneisses. We note that the formational age of TTG gneiss found in our study (~2.7–2.6 Ga) is older than an age of ~2.5 Ga obtained by Zhang et al. (2013b) in the southern margin of the Dunhuang block. Furthermore, the oldest TTG gneiss in the Kuluketage block on the northern margin of the Tarim craton formed 2.65 Ga ago (Long et al., 2011); this gneiss exhibits Hf isotope compositions similar to those in one sample in our study (X11-114-1 with an age of 2.64 ± 0.06 Ga) (Fig. 8). Similarly, tonalite with an age of ~2.6 Ga was also reported by Zhang et al. (2012a) in

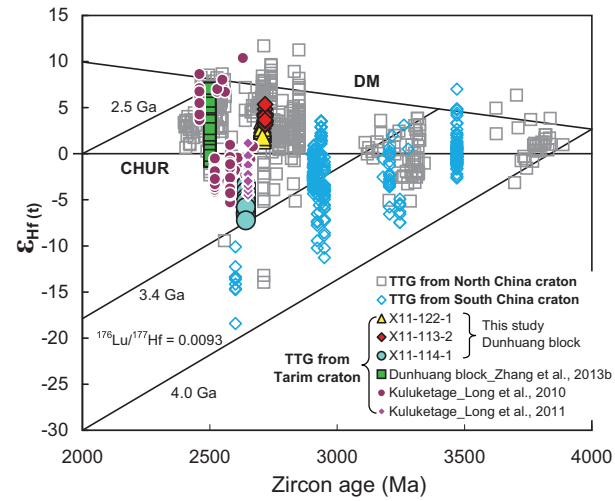

Fig. 8. Plot of $\varepsilon_{Hf}(t)$ values versus zircon formation ages of TTG gneiss in the Dunhuang block. Published data of TTG gneiss in the Tarim craton (Long et al., 2010, 2011; Zhang et al., 2013b), North China craton (Diwu et al., 2010, 2011; Huang et al., 2010; Jiang et al., 2010; Liu et al., 2009a, 2012a; Wan et al., 2011; Wu et al., 2008; Zhang et al., 2013a) and South China craton (Chen et al., 2013; Gao et al., 2011; Guo et al., 2013; Zhang et al., 2006) are shown for comparison.

the Kuluketage block. Considering ~2.5 Ga TTG gneisses and granites in the Kuluketage (Long et al., 2010; Zhang et al., 2012a), we suggest that both the Kuluketage and Dunhuang blocks underwent two-stage (~2.7–2.6 Ga and ~2.5 Ga ago) intrusion of Neoarchean TTG in the Tarim craton. In contrast, TTG gneisses and associated granitoid rocks with ages of ~2.7–2.6 Ga have also been found during recent studies in both the North China and South China cratons (Chen et al., 2013; Huang et al., 2010; Jiang et al., 2010; Wu et al., 2013; Zhao et al., 2007; Zhao and Zhai, 2013; Zheng et al., 2013). The conclusion that such episodic events occurred ~2.7–2.6 Ga and ~2.5 Ga ago in the evolution of Archean continental crust has been supported by syntheses of global zircon U–Pb dating of modern river sediments and orogenic granitoids (Condie and Aster, 2010; Condie et al., 2009, 2011).

Archean TTG gneisses always exhibit analogous compositions with adakite (Martin, 1999). Martin et al. (2005) further subdivided adakitic rocks into high SiO_2 adakites (HSA) and low SiO_2 adakites (LSA) on the basis of silicon content. HSA derived from partial melting of basaltic slab are always characterized by high SiO_2 (>60%) and low MgO (0.5–4%), CaO + Na_2O (<11 wt%) and Sr (<1100 ppm) contents, which is more similar to global TTG gneisses than LSA (Martin et al., 2005). Neoarchean TTG gneisses in this study have consistent geochemical compositions with HAS, but the very low Cr (6.5–11.2 ppm) and Ni (6.3–11.1) contents suggest that these TTG magma could be resulted from partial melting of subducted slab without interaction with peridotite in the mantle wedge (Martin et al., 2005; Rapp et al., 1999).

5.2. Implication for the Archean continental crustal growth in the Tarim craton

The growth of the crust is a process that is a direct result of extraction of mafic melt from the mantle (Cawood et al., 2013; Hawkesworth et al., 2010; Rudnick, 1995). Thus, the generation of felsic TTG gneiss cannot be considered to be the real source of growth of continental crust. However, the ages of crust generation can be inferred from zircon Hf isotope model ages of felsic rocks (Amelin et al., 1999; Griffin et al., 2004; Hawkesworth et al., 2010). In our study, magmatic zircon cores with ages of ~2.7–2.6 Ga from two TTG gneisses (X11-113-2 and X11-122-1) show positive $\varepsilon_{Hf}(t)$

Table 3
Lu–Hf isotope compositions of zircons from the TTG gneisses in the Dunhuang block, northeastern Tarim craton[a].

Spot No.	$^{176}Hf/^{177}Hf$	1σ	$^{176}Lu/^{177}Hf$	1σ	$^{176}Yb/^{177}Hf$	1σ (X11-113-2)	Age (Ma)	$^{176}Hf/^{177}Hf(t)$	$\varepsilon_{Hf}(t)$	1σ	T_{DM1}	T_{DM2}	$f_{Lu/Hf}$
04	0.281146	0.000012	0.000247	0.000021	0.009158	0.000686	1914	0.281137	−15.2	0.8	2.88	3.28	−0.99
06	0.281150	0.000010	0.000203	0.000006	0.007635	0.000191	1914	0.281142	−15.0	0.7	2.87	3.27	−0.99
08	0.281150	0.000010	0.000092	0.000001	0.004268	0.000066	1914	0.281147	−14.9	0.7	2.86	3.26	−1.00
12	0.281139	0.000010	0.000117	0.000007	0.005255	0.000233	1914	0.281134	−15.3	0.7	2.88	3.29	−1.00
16	0.281148	0.000013	0.000296	0.000016	0.011005	0.000590	1914	0.281137	−15.2	0.8	2.88	3.28	−0.99
18	0.281198	0.000008	0.000378	0.000028	0.014934	0.000981	1914	0.281184	−13.6	0.7	2.82	3.19	−0.99
22	0.281141	0.000009	0.000230	0.000005	0.006904	0.000080	1914	0.281133	−15.4	0.7	2.88	3.29	−0.99
25	0.281179	0.000014	0.000170	0.000003	0.006602	0.000063	1914	0.281173	−13.9	0.8	2.83	3.21	−0.99
26	0.281171	0.000011	0.000455	0.000021	0.017081	0.000759	1914	0.281155	−14.6	0.8	2.86	3.25	−0.99
32	0.281146	0.000010	0.000221	0.000007	0.008480	0.000202	1914	0.281138	−15.2	0.7	2.87	3.28	−0.99
33	0.281181	0.000012	0.000565	0.000043	0.021512	0.001652	1914	0.281161	−14.4	0.8	2.85	3.24	−0.98
34	0.281140	0.000012	0.000451	0.000026	0.017096	0.000924	1914	0.281124	−15.7	0.8	2.90	3.31	−0.99
38	0.281144	0.000010	0.000258	0.000022	0.009217	0.000764	1914	0.281134	−15.3	0.7	2.88	3.29	−0.99
39	0.281168	0.000012	0.000324	0.000003	0.011789	0.000068	1914	0.281156	−14.5	0.8	2.85	3.25	−0.99
41	0.281182	0.000012	0.000383	0.000039	0.015228	0.001395	1914	0.281168	−14.1	0.8	2.84	3.22	−0.99
42	0.281153	0.000008	0.000261	0.000013	0.009733	0.000474	1914	0.281144	−15.0	0.7	2.87	3.27	−0.99
44	0.281182	0.000012	0.000485	0.000024	0.017520	0.000827	1914	0.281164	−14.3	0.8	2.85	3.23	−0.99
01	0.281195	0.000009	0.000544	0.000020	0.020384	0.000741	2717	0.281167	4.3	0.8	2.83	2.88	−0.98
02	0.281188	0.000008	0.000450	0.000023	0.016769	0.000964	2717	0.281165	4.2	0.8	2.83	2.88	−0.99
03	0.281175	0.000012	0.000336	0.000005	0.012210	0.000251	2717	0.281157	4.0	0.8	2.84	2.90	−0.99
05	0.281156	0.000009	0.000193	0.000010	0.006920	0.000392	2717	0.281146	3.6	0.8	2.86	2.92	−0.99
07	0.281158	0.000012	0.000328	0.000013	0.011888	0.000518	2717	0.281141	3.4	0.8	2.87	2.93	−0.99
09	0.281149	0.000014	0.000299	0.000009	0.011068	0.000290	2717	0.281134	3.1	0.9	2.87	2.94	−0.99
14	0.281153	0.000008	0.000170	0.000003	0.005720	0.000105	2717	0.281144	3.5	0.8	2.86	2.92	−0.99
15	0.281193	0.000011	0.000505	0.000004	0.018719	0.000161	2717	0.281166	4.3	0.8	2.83	2.88	−0.98
17	0.281193	0.000010	0.000613	0.000023	0.023682	0.000832	2717	0.281161	4.1	0.8	2.84	2.89	−0.98
21	0.281189	0.000012	0.000431	0.000004	0.015557	0.000160	2717	0.281166	4.3	0.8	2.83	2.88	−0.99
23	0.281163	0.000012	0.000289	0.000004	0.011268	0.000223	2717	0.281148	3.6	0.8	2.86	2.91	−0.99
27	0.281162	0.000010	0.000482	0.000017	0.018278	0.000729	2717	0.281137	3.2	0.8	2.87	2.94	−0.99
29	0.281207	0.000009	0.000484	0.000008	0.018031	0.000372	2717	0.281182	4.8	0.8	2.81	2.85	−0.99
30	0.281191	0.000010	0.000439	0.000008	0.016497	0.000253	2717	0.281168	4.3	0.8	2.83	2.88	−0.99
31	0.281186	0.000008	0.000440	0.000012	0.016115	0.000563	2717	0.281164	4.2	0.8	2.84	2.88	−0.99
35	0.281167	0.000012	0.000386	0.000014	0.015652	0.000696	2717	0.281147	3.6	0.8	2.86	2.92	−0.99
37	0.281182	0.000009	0.000369	0.000023	0.013705	0.000958	2717	0.281162	4.1	0.8	2.84	2.89	−0.99
40	0.281218	0.000009	0.000408	0.000011	0.015050	0.000347	2717	0.281197	5.4	0.8	2.79	2.82	−0.99
46	0.281175	0.000014	0.000500	0.000012	0.018334	0.000405	2717	0.281149	3.7	0.9	2.85	2.91	−0.98
Spot No.	$^{176}Hf/^{177}Hf$	1σ	$^{176}Lu/^{177}Hf$	1σ	$^{176}Yb/^{177}Hf$	1σ (X11-114-1)	Age (Ma)	$^{176}Hf/^{177}Hf(t)$	$\varepsilon_{Hf}(t)$	1σ	T_{DM1}	T_{DM2}	$f_{Lu/Hf}$
09	0.281508	0.000018	0.000646	0.000008	0.020869	0.000361	417	0.281503	−35.7	0.8	2.42	3.23	−0.98
18	0.281701	0.000014	0.000570	0.000009	0.017369	0.000270	417	0.281697	−28.9	0.7	2.15	2.86	−0.98
21	0.281442	0.000045	0.001850	0.000024	0.052386	0.000650	417	0.281427	−38.4	1.7	2.59	3.37	−0.94
34	0.281442	0.000071	0.001850	0.000059	0.052386	0.001391	417	0.281427	−38.4	2.6	2.59	3.37	−0.94
04	0.281163	0.000009	0.002034	0.000033	0.078336	0.001758	2002	0.281085	−15.0	0.7	2.99	3.34	−0.94
11	0.281003	0.000009	0.000479	0.000005	0.016671	0.000221	2002	0.280984	−18.6	0.7	3.08	3.53	−0.99
15	0.281140	0.000018	0.001244	0.000033	0.047575	0.001818	2002	0.281092	−14.8	0.9	2.96	3.33	−0.96
16	0.281042	0.000009	0.000114	0.000003	0.004361	0.000100	2002	0.281037	−16.8	0.7	3.00	3.43	−1.00
17	0.280992	0.000013	0.000439	0.000036	0.014910	0.001188	2002	0.280976	−18.9	0.8	3.09	3.55	−0.99
19	0.281076	0.000007	0.000236	0.000028	0.009279	0.001053	2002	0.281067	−15.7	0.7	2.97	3.38	−0.99
22	0.280979	0.000013	0.001035	0.000011	0.034835	0.000427	2002	0.280940	−20.2	0.8	3.16	3.62	−0.97
28	0.281053	0.000010	0.000442	0.000022	0.015771	0.000652	2002	0.281037	−16.8	0.7	3.01	3.43	−0.99
33	0.281089	0.000008	0.000174	0.000008	0.006261	0.000282	2002	0.281082	−15.2	0.7	2.95	3.35	−0.99
03	0.280961	0.000013	0.000879	0.000024	0.029967	0.000862	2642	0.280917	−6.3	0.9	3.17	3.38	−0.97
05	0.280991	0.000013	0.001217	0.000023	0.042917	0.000893	2642	0.280930	−5.9	0.9	3.16	3.36	−0.96
07	0.281037	0.000011	0.000748	0.000034	0.026236	0.001028	2642	0.281000	−3.4	0.8	3.06	3.23	−0.98
07R	0.281042	0.000010	0.000846	0.000059	0.029908	0.001945	2642	0.280999	−3.4	0.8	3.06	3.23	−0.97
10	0.281037	0.000012	0.001195	0.000041	0.043103	0.001411	2642	0.280977	−4.2	0.9	3.09	3.27	−0.96
12	0.281018	0.000012	0.001341	0.000062	0.046521	0.002136	2642	0.280951	−5.1	0.9	3.13	3.32	−0.96
13	0.280973	0.000012	0.001142	0.000079	0.039026	0.002570	2642	0.280915	−6.4	0.9	3.18	3.39	−0.97
14	0.280961	0.000012	0.000948	0.000025	0.031537	0.001143	2642	0.280913	−6.5	0.8	3.18	3.39	−0.97
20	0.281028	0.000012	0.001002	0.000021	0.034789	0.000684	2642	0.280978	−4.2	0.8	3.09	3.27	−0.97
23	0.281039	0.000013	0.001176	0.000077	0.040901	0.002589	2642	0.280979	−4.1	0.9	3.09	3.27	−0.96
24	0.280953	0.000009	0.000836	0.000020	0.028706	0.000665	2642	0.280911	−6.6	0.8	3.18	3.39	−0.97
25	0.280972	0.000014	0.001343	0.000080	0.045940	0.002666	2642	0.280904	−6.8	0.9	3.20	3.41	−0.96
26	0.280971	0.000012	0.001235	0.000057	0.043403	0.001932	2642	0.280909	−6.6	0.9	3.19	3.40	−0.96
27	0.281013	0.000012	0.001586	0.000108	0.055674	0.003701	2642	0.280933	−5.8	0.9	3.16	3.35	−0.95
29	0.281016	0.000012	0.001131	0.000067	0.040423	0.002348	2642	0.280959	−4.8	0.9	3.12	3.30	−0.97
30	0.281013	0.000010	0.001267	0.000018	0.044215	0.000745	2642	0.280949	−5.2	0.8	3.13	3.32	−0.96
31	0.281006	0.000010	0.001459	0.000068	0.050367	0.002225	2642	0.280932	−5.8	0.8	3.16	3.35	−0.96
32	0.280957	0.000011	0.001298	0.000040	0.044958	0.001278	2642	0.280892	−7.2	0.8	3.21	3.43	−0.96
Spot No.	$^{176}Hf/^{177}Hf$	1σ	$^{176}Lu/^{177}Hf$	1σ	$^{176}Yb/^{177}Hf$	1σ (X11-122-1)	Age (Ma)	$^{176}Hf/^{177}Hf(t)$	$\varepsilon_{Hf}(t)$	1σ	T_{DM1}	T_{DM2}	$f_{Lu/Hf}$
31	0.281669	0.000017	0.000197	0.000015	0.007842	0.000545	430	0.281668	−29.6	0.8	2.17	2.91	−0.99
31R	0.281613	0.000012	0.000147	0.000005	0.005951	0.000250	430	0.281612	−31.6	0.7	2.24	3.02	−1.00
35R	0.281719	0.000007	0.000155	0.000004	0.005879	0.000198	430	0.281717	−27.9	0.6	2.10	2.82	−1.00
35	0.281789	0.000011	0.000248	0.000013	0.009316	0.000543	430	0.281787	−25.4	0.7	2.01	2.68	−0.99

Table 3 (*Continued*).

Spot No.	$^{176}Hf/^{177}Hf$	1σ	$^{176}Lu/^{177}Hf$	1σ	$^{176}Yb/^{177}Hf$	1σ (X11-122-1)	Age (Ma)	$^{176}Hf/^{177}Hf$ (*t*)	$\varepsilon_{Hf}(t)$	1σ	T_{DM1}	T_{DM2}	$f_{Lu/Hf}$
14	0.281272	0.000011	0.000414	0.000017	0.014908	0.000519	1966	0.281256	−9.8	0.8	2.72	3.03	−0.99
17	0.281158	0.000010	0.000392	0.000035	0.013625	0.001150	1966	0.281143	−13.8	0.8	2.87	3.25	−0.99
18	0.281190	0.000008	0.000203	0.000019	0.008260	0.000698	1966	0.281183	−12.4	0.7	2.81	3.17	−0.99
22	0.281280	0.000012	0.000264	0.000003	0.008678	0.000051	1966	0.281270	−9.3	0.8	2.70	3.01	−0.99
24	0.281141	0.000015	0.000461	0.000007	0.017273	0.000270	1966	0.281124	−14.5	0.8	2.90	3.28	−0.99
28	0.281136	0.000008	0.000180	0.000001	0.007187	0.000035	1966	0.281130	−14.3	0.7	2.88	3.27	−0.99
33	0.281237	0.000016	0.000322	0.000024	0.011680	0.000617	1966	0.281225	−10.9	0.9	2.76	3.09	−0.99
36	0.281206	0.000007	0.000212	0.000011	0.007708	0.000409	1966	0.281198	−11.9	0.7	2.79	3.14	−0.99
40	0.281176	0.000011	0.000535	0.000028	0.019484	0.000932	1966	0.281156	−13.4	0.8	2.86	3.22	−0.98
41	0.281189	0.000009	0.000205	0.000009	0.008239	0.000431	1966	0.281182	−12.4	0.7	2.81	3.17	−0.99
43	0.281193	0.000009	0.000221	0.000009	0.009093	0.000410	1966	0.281185	−12.3	0.7	2.81	3.17	−0.99
47	0.281332	0.000010	0.000552	0.000010	0.022766	0.000587	1966	0.281311	−7.8	0.7	2.65	2.93	−0.98
47R	0.281321	0.000009	0.000781	0.000004	0.033813	0.000364	1966	0.281292	−8.5	0.7	2.68	2.97	−0.98
01	0.281133	0.000008	0.000186	0.000004	0.006465	0.000173	2707	0.281124	2.5	0.8	2.89	2.96	−0.99
03	0.281121	0.000008	0.000336	0.000019	0.011283	0.000543	2707	0.281103	1.8	0.8	2.92	3.00	−0.99
04	0.281151	0.000011	0.000654	0.000010	0.023659	0.000540	2707	0.281117	2.3	0.8	2.90	2.98	−0.98
06	0.281147	0.000010	0.000974	0.000070	0.034609	0.002488	2707	0.281097	1.6	0.9	2.93	3.02	−0.97
07	0.281157	0.000010	0.000532	0.000016	0.018853	0.000680	2707	0.281130	2.7	0.8	2.88	2.95	−0.98
10	0.281130	0.000012	0.000338	0.000012	0.011578	0.000468	2707	0.281113	2.1	0.8	2.90	2.98	−0.99
11	0.281150	0.000008	0.000569	0.000017	0.019682	0.000492	2707	0.281120	2.4	0.8	2.89	2.97	−0.98
13	0.281152	0.000008	0.000423	0.000010	0.014232	0.000275	2707	0.281130	2.7	0.8	2.88	2.95	−0.99
16	0.281161	0.000012	0.000135	0.000003	0.005435	0.000176	2707	0.281154	3.6	0.8	2.85	2.91	−1.00
20	0.281138	0.000009	0.000442	0.000015	0.015308	0.000523	2707	0.281115	2.2	0.8	2.90	2.98	−0.99
21	0.281126	0.000011	0.000448	0.000008	0.015521	0.000348	2707	0.281103	1.8	0.8	2.92	3.00	−0.99
23	0.281180	0.000010	0.000740	0.000033	0.027534	0.001326	2707	0.281142	3.2	0.8	2.87	2.93	−0.98
25	0.281160	0.000008	0.000488	0.000021	0.018451	0.000844	2707	0.281135	2.9	0.8	2.87	2.94	−0.99
32	0.281140	0.000009	0.000511	0.000021	0.018254	0.000836	2707	0.281114	2.2	0.8	2.90	2.98	−0.98
37	0.281142	0.000010	0.000277	0.000005	0.009722	0.000305	2707	0.281128	2.7	0.8	2.88	2.96	−0.99
38	0.281153	0.000008	0.000620	0.000029	0.022714	0.001195	2707	0.281121	2.4	0.8	2.89	2.97	−0.98
39	0.281129	0.000008	0.000668	0.000015	0.025009	0.000655	2707	0.281094	1.5	0.8	2.93	3.02	−0.98
44	0.281157	0.000008	0.000613	0.000040	0.022220	0.001423	2707	0.281125	2.6	0.8	2.89	2.96	−0.98
48	0.281163	0.000012	0.000594	0.000021	0.021447	0.000801	2707	0.281132	2.8	0.8	2.88	2.95	−0.98
49	0.281120	0.000010	0.000314	0.000007	0.011153	0.000256	2707	0.281104	1.8	0.8	2.92	3.00	−0.99

[a] $^{176}Hf/^{177}Hf$ (*t*) represents initial $^{176}Hf/^{177}Hf$ ratio of zircon. ε_{Hf} (*t*) is calculated relative to a chondritic reservoir with a present-day $^{176}Hf/^{177}Hf$ ratio of 0.282772 and $^{176}Lu/^{177}Hf$ ratio of 0.0332. Present-day $^{176}Hf/^{177}Hf$ ratio of 0.28325 and $^{176}Lu/^{177}Hf$ ratio of 0.0384 for depleted mantle (Griffin et al., 2000) and a mean value of $^{176}Lu/^{177}Hf$ ratio of 0.0093 for the upper continental crust (Vervoort and Jonathan Patchett, 1996) were used during calculation of T_{DM1} and T_{DM2}.

values of 1.5–5.4 and relatively young two-stage Hf isotope model ages of ~3.0–2.9 Ga, suggesting that the juvenile Mesoarchean crust in the Dunhuang block was reworked in the Neoarchean Era. This is consistent with that Mesoarchean two-stage Nd isotope model ages of ~3.06–2.84 Ga were obtained for these samples (Table 2). However, negative ε_{Hf} (*t*) values ranging from –3.4 to –7.2 and relatively older two-stage Hf isotope model ages of 3.4–3.2 Ga were given by ages of ~2.7 Ga of magmatic zircon cores in one sample (X11-114-2), indicating that Paleoarchean continental crust material as old as 3.4 Ga could be present in the Dunhuang block and it was reworked in the Neoarchean. We note that the peak Hf isotope model ages are between ~2.95 Ga and 3.4 Ga for magmatic zircon cores with ages of ~2.7–2.6 Ga from the TTG gneiss in this study (Fig. 9b). Meanwhile, a ~2.8 Ga peak zircon Hf isotope model age of Archean TTG gneiss has been obtained by Zhang et al. (2013b) in the southern margin of the Dunhuang block (Fig. 9b). Furthermore, the peak zircon Hf isotope model ages of Archean TTG gneiss in the Kuluketage block on the northern margin of Tarim craton are ~2.6 Ga and ~3.2 Ga (Long et al., 2011, 2010) (Fig. 9b). After combining our results with all of these studies, we suggest that the Tarim craton could have experienced episodic generation of juvenile continental crust during the Paleoarchean to Neoarchean Eras (~3.4 Ga, ~3.2 Ga, ~2.95 Ga, ~2.8 Ga and ~2.6 Ga) (Fig. 9b).

On the basis of all published zircon Hf isotope data of Archean TTG gneisses from the North China, South China and Tarim cratons, we note that the North China craton experienced a prolong generation of Archean continent crust ranging from ~4.0 Ga to ~2.5 Ga and the peak ages are ~3.1 Ga and ~2.75 Ga. While, the Archean crustal growth in the South China craton varied from ~4.0 Ga to ~3.1 Ga and the peak ages are ~3.4 Ga and ~3.7 Ga (Fig. 9a). Thus, we suggest that the Meoarchean and Neoarchean Eras are the main periods for generation of Archean continental crust in the North China and Tarim cratons, and Eoarchean and Paleoarchean Eras are the main periods for generation of Archean continental crust in the South China craton.

5.3. Paleoproterozoic and Paleozoic tectonothermal overprints on Archean TTG in the Tarim craton

The CL images from our study revealed that most zircon mantle/cores with ages of ~2.0–1.9 Ga and outermost zircon rims with ages of ~430 Ma exhibit homogenous CL images (Fig. 6), which are always observed in metamorphic zircons (Corfu et al., 2003). In contrast, some zircon mantle/cores with ages of ~2.0–1.9 Ga show flat HREE patterns and negative Eu anomalies (Fig. 7 b and d), suggesting these zircon domains are in equilibrium with garnet and plagioclase during growth at high-grade metamorphism (Hoskin and Schaltegger, 2003; Rubatto, 2002). This finding is consistent with the presence of garnet-bearing felsic vein in such TTG gneisses, in which ~2.0–1.9-Ga-old metamorphic zircon grains can be identified (our unpublished data). The outermost zircon rims with ages of ~430 Ma are characterized by very steep HREE patterns, neglected Eu anomalies and very low Th/U ratios (0.001–0.03) (Fig. 7 d, f and Supplementary Tables 2–3), which are always observed in anatectic zircon resulting from high-grade metamorphism (Liu et al., 2012c). The metamorphic zircon mantle/cores with ages of ~2.0–1.9 Ga show initial $^{176}Hf/^{177}Hf$ ratios consistent with those of inherited magmatic zircon cores with ages of ~2.7–2.6 Ga, while outermost zircon rims with ages of ~430 Ma have obviously higher initial $^{176}Hf/^{177}Hf$ ratios compared to other domains, indicating that ~2.0–1.9-Ga-old zircon formed by the dissolution-reprecipitation of pre-existing ~2.7–2.6-Ga-old inherited zircon in a closed system and that ~430-Ma-old new-growth zircon domains were re-equilibrated with their matrix in an open

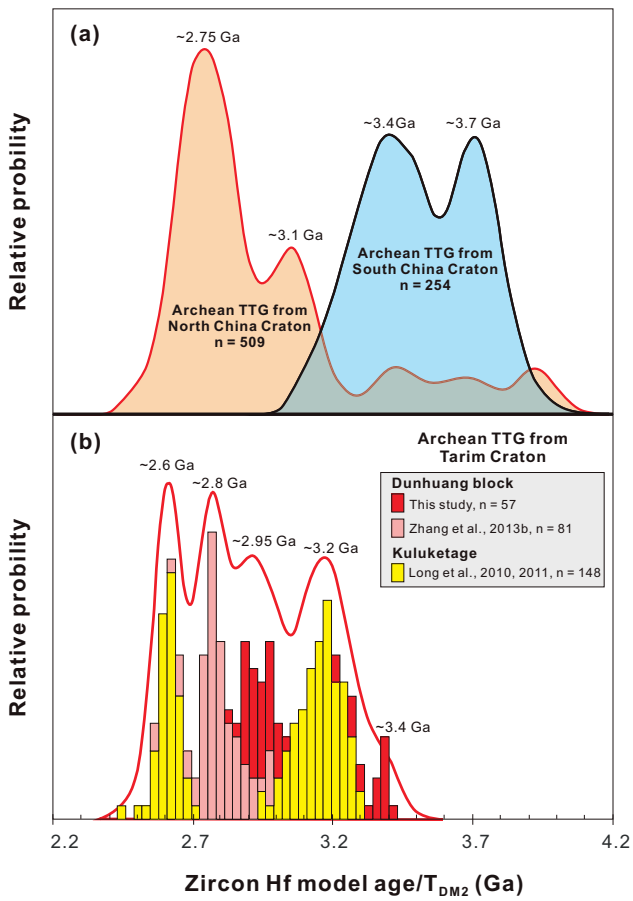

Fig. 9. Relative probability plot of two-stage Hf crust formation model ages for zircons in Archean TTG gneisses from the Tarim craton, North China craton (Diwu et al., 2010, 2011; Huang et al., 2010; Jiang et al., 2010; Liu et al., 2009a, 2012a; Wan et al., 2011; Wu et al., 2008; Zhang et al., 2013a) and South China craton (Chen et al., 2013; Gao et al., 2011; Guo et al., 2013; Zhang et al., 2006).

system (Gerdes and Zeh, 2009; Liu et al., 2012b; Wu et al., 2007). Therefore, we suggest that the Archean continental crust in the Dunhuang block has undergone two-stage Paleoproterozoic and Paleozoic tectonothermal events. This conclusion is consistent with the findings of Paleoproterozoic and early Paleozoic high-pressure granulite metamorphism in the Dunhuang block (Zhang et al., 2012c; Zong et al., 2012), which were interpreted as an assembly of the Columbia supercontinent (Zhang et al., 2012c) and early Paleozoic continental collision (Zong et al., 2012), respectively. However, we note that Paleoproterozoic age of ~2.0–1.9 Ga obtained in this study is obviously older than ~1.85 Ga age of high pressure granulite metamorphism reported by Zhang et al. (2012c). This possibly reflects another Paleoproterozoic tectonothermal event and the south and the interior of the Dunhuang block could have been suffered from different Paleoproterozoic metamorphic evolution. Furthermore, Paleoproterozoic metamorphic and early Paleozoic magmatic events were also prevalent in the Kuluketage block on the northern margin of the Tarim craton (Ge et al., 2012; Long et al., 2010; Zhang et al., 2012b). Thus, the whole Archean basement in the Tarim craton could have been subjected to Paleoproterozoic and Paleozoic tectonothermal overprinting.

6. Conclusions

Geochemical and geochronological signatures of three typical Archean TTG gneisses in the Dunhuang block were reported and characterized to constrain the generation and evolution of the Archean continental crust in the Tarim craton. TTG gneisses in the interior of the Dunhuang block formed ~2.7–2.6 Ga ago, which can be considered a time of reworking of the Paleoarchean (~3.4 Ga) and Mesoarchean (~2.95 Ga) juvenile continental crust. This study also revealed that Neoarchean TTG gneisses in the Dunhuang block have been subjected to Paleoproterozoic and early Paleozoic tectonothermal alteration. Lastly, based on our analyses of and correlations with previous studies, we suggest that the Tarim craton could have experienced two-stage (~2.7–2.6 Ga and ~2.5 Ga) intrusion of TTG and episodic (~3.4 Ga, ~3.2 Ga, ~2.95 Ga, ~2.8 Ga and ~2.6 Ga) generation of Archean continental crust.

Acknowledgements

We are most grateful to Prof. Jianxin Zhang and an anonymous reviewer for critical and constructive reviews of the original manuscript. This research is co-supported by the Chinese Geological Survey Project (1212011085478, 1212011120161), the Special Research Fund from the Ministry of Land and Resources of China (201011034), the National Natural Science Foundation of China (90914007 and 41125013, 41203027,), the State Administration of Foreign Expert Affairs of China (B07039), the Research Fund for the Doctoral Program of Higher Education of China (2011014512), the Special Fund for Basic Scientific Research of Central Colleges, China University of Geosciences (Wuhan) (CUG090105 and CUGL110207) and MOST Special Fund of State Key Laboratory of Geological Processes and Mineral Resources (MSFGPMR201204).

References

Amelin, Y., Lee, D.-C., Halliday, A.N., Pidgeon, R.T., 1999. Nature of the Earth's earliest crust from hafnium isotopes in single detrital zircons. Nature 399, 252–255.
Barker, F., 1979. Trondhjemites: definition environment and hypothesis of origin. In: Barker, F. (Ed.), Trondhjemites, Dacites and Related Rocks. Elsevier, Amsterdam, pp. 1–12.
Cawood, P.A., Hawkesworth, C.J., Dhuime, B., 2013. The continental record and the generation of continental crust. Geological Society of America Bulletin 125, 14–32.
Chen, K., Gao, S., Wu, Y.B., Guo, J.L., Hu, Z.C., Liu, Y.S., Zong, K.Q., Liang, Z.W., Geng, X.L., 2013. 2.6–2.7 Ga crustal growth in Yangtze craton South China. Precambrian Research 224, 472–490.
Chen, Y., Xu, B., Zhan, S., Li, Y., 2004. First mid-Neoproterozoic paleomagnetic results from the Tarim Basin (NW China) and their geodynamic implications. Precambrian Research 133, 271–281.
Condie, K.C., 2005. Earth as an Evolving Planetary System. Elservier, Burlington.
Condie, K.C., Aster, R.C., 2010. Episodic zircon age spectra of orogenic granitoids: the supercontinent connection and continental growth. Precambrian Research 180, 227–236.
Condie, K.C., Belousova, E., Griffin, W.L., Sircombe, K.N., 2009. Granitoid events in space and time: constraints from igneous and detrital zircon age spectra. Gondwana Research 15, 228–242.
Condie, K.C., Bickford, M.E., Aster, R.C., Belousova, E., Scholl, D.W., 2011. Episodic zircon ages, Hf isotopic composition, and the preservation rate of continental crust. Geological Society of America Bulletin 123, 951–957.
Condie, K.C., Kröner, A., 2013. The building blocks of continental crust: evidence for a major change in the tectonic setting of continental growth at the end of the Archean. Gondwana Research 23, 394–402.
Corfu, F., 2013. A century of U–Pb geochronology: the long quest towards concordance. Geological Society of America Bulletin 125, 33–47.
Corfu, F., Hanchar, J.M., Hoskin, P.W.O., Kinny, P., 2003. Atlas of zircon textures. Reviews in Mineralogy and Geochemistry 53, 469–500.
Diwu, C.R., Sun, Y., Guo, A.L., Wang, H.L., Liu, X.M., 2011. Crustal growth in the North China Craton at ~2.5 Ga: evidence from in situ zircon U–Pb ages, Hf isotopes and whole-rock geochemistry of the Dengfeng complex. Gondwana Research 20, 149–170.
Diwu, C.R., Sun, Y., Lin, C.L., Wang, H.L., 2010. LA–(MC)–ICPMS U–Pb zircon geochronology and Lu–Hf isotope compositions of the Taihua complex on the southern margin of the North China Craton. Chinese Science Bulletin 55, 2557–2571.
Gao, S., Rudnick, R.L., Yuan, H.L., Liu, X.M., Liu, Y.S., Xu, W.L., Ling, W.L., Ayers, J., Wang, X.C., Wang, Q.H., 2004. Recycling lower continental crust in the North China craton. Nature 432, 892–897.
Gao, S., Yang, J., Zhou, L., Li, M., Hu, Z., Guo, J., Yuan, H., Gong, H., Xiao, G., Wei, J., 2011. Age and growth of the Archean Kongling terrain, South China, with emphasis on 3.3 Ga granitoid gneisses. American Journal of Science 311, 153–182.

Ge, R.F., Zhu, W.B., Wu, H.L., Zheng, B.H., Zhu, X.Q., He, J.W., 2012. The Paleozoic northern margin of the Tarim Craton: passive or active? Lithos 142–143, 1–15.
Gerdes, A., Zeh, A., 2009. Zircon formation versus zircon alteration-new insights from combined U–Pb and Lu–Hf in-situ LA–ICP–MS analyses, and consequences for the interpretation of Archean zircon from the Central Zone of the Limpopo Belt. Chemical Geology 261, 230–243.
Griffin, W.L., Belousova, E.A., Shee, S.R., Pearson, N.J., O'Reilly, S.Y., 2004. Archean crustal evolution in the northern Yilgarn Craton: U–Pb and Hf-isotope evidence from detrital zircons. Precambrian Research 131, 231–282.
Griffin, W.L., Pearson, N.J., Belousova, E., Jackson, S.E., van Achterbergh, E., O'Reilly, S.Y., Shee, S.R., 2000. The Hf isotope composition of cratonic mantle: LAM–MC–ICPMS analysis of zircon megacrysts in kimberlites. Geochimica et Cosmochimica Acta 64, 133–147.
Guo, J.L., Gao, S., Wu, Y.B., Li, M., CHen, K., Liu, Y.S., Hu, Z.C., Zhou, L., 2013. ≥3.47 Ga granitic gneisses from the Yangtze Craton, South China: implications for the Early Archean crustal growth. Precambrian Research. (in review).
Hawkesworth, C.J., Dhuime, B., Pietranik, A.B., Cawood, P.A., Kemp, A.I.S., Storey, C.D., 2010. The generation and evolution of the continental crust. Journal of the Geological Society 167, 229–248.
Hoskin, P.W.O., Schaltegger, U., 2003. The composition of zircon and igneous and metamorphic petrogenesis. Reviews in Mineralogy and Geochemistry 53, 27–62.
Hu, Z.C., Gao, S., Liu, Y.S., Hu, S.H., Chen, H.H., Yuan, H.L., 2008a. Signal enhancement in laser ablation ICP–MS by addition of nitrogen in the central channel gas. Journal of Analytical Atomic Spectrometry 23, 1093–1101.
Hu, Z.C., Liu, Y.S., Gao, S., Hu, S.H., Dietiker, R., Günther, D., 2008b. A local aerosol extraction strategy for the determination of the aerosol composition in laser ablation inductively coupled plasma mass spectrometry. Journal of Analytical Atomic Spectrometry 23, 1192–1203.
Hu, Z.C., Liu, Y.S., Gao, S., Liu, W.G., Zhang, W., Tong, X.R., Lin, L., Zong, K.Q., Li, M., Chen, H.H., Zhou, L., Yang, L., 2012. Improved in situ Hf isotope ratio analysis of zircon using newly designed X skimmer cone and jet sample cone in combination with the addition of nitrogen by laser ablation multiple collector ICP–MS. Journal of Analytical Atomic Spectrometry 27, 1391–1399.
Huang, X.L., Niu, Y.L., Xu, Y.G., Yang, Q.J., Zhong, J.W., 2010. Geochemistry of TTG and TTG-like gneisses from Lushan–Taihua complex in the southern North China Craton: implications for late Archean crustal accretion. Precambrian Research 182, 43–56.
Jackson, S.E., Pearson, N.J., Griffin, W.L., Belousova, E.A., 2004. The application of laser ablation-inductively coupled plasma-mass spectrometry to in situ U–Pb zircon geochronology. Chemical Geology 211, 47–69.
Jiang, N., Guo, J.H., Zhai, M.G., Zhang, S.Q., 2010. ~2.7 Ga crust growth in the North China craton. Precambrian Research 179, 37–49.
Liou, J.G., Graham, S.A., Maruyama, S., Zhang, R.Y., 1996. Characteristics and tectonic significance of the late Proterozoic Aksu blueschists and diabasic dikes, Northwest Xinjiang, China. International Geology Review 38, 228–244.
Liu, D.Y., Wilde, S.A., Wan, Y.S., Wang, S.Y., Valley, J.W., Kita, N., Dong, C.Y., Xie, H.Q., Yang, C.X., Zhang, Y.X., Gao, L.Z., 2009a. Combined U–Pb, hafnium and oxygen isotope analysis of zircons from meta-igneous rocks in the southern North China Craton reveal multiple events in the Late Mesoarchean–Early Neoarchean. Chemical Geology 261, 140–154.
Liu, F., Guo, J.H., Peng, P., Qian, Q., 2012a. Zircon U–Pb ages and geochemistry of the Huai'an TTG gneisses terrane: petrogenesis and implications for ~2.5 Ga crustal growth in the North China Craton. Precambrian Research 212–213, 225–244.
Liu, F.L., Gerdes, A., Liu, P.H., 2012b. U–Pb, trace element and Lu–Hf properties of unique dissolution–reprecipitation zircon from UHP eclogite in SW Sulu terrane, eastern China. Gondwana Research 22, 169–183.
Liu, F.L., Robinson, P.T., Liu, P.H., 2012c. Multiple partial melting events in the Sulu UHP terrane: zircon U–Pb dating of granitic leucosomes within amphibolite and gneiss. Journal of Metamorphic Geology 10, 1111/j.1525-1314.2012.01005.x.
Liu, Y.S., Gao, S., Hu, Z.C., Gao, C.G., Zong, K.Q., Wang, D.B., 2010a. Continental and oceanic crust recycling-induced melt-peridotite interactions in the Trans-North China Orogen: U–Pb dating, Hf isotopes and trace elements in zircons from mantle xenoliths. Journal of Petrology 51, 537–571.
Liu, Y.S., Hu, Z.C., Gao, S., Günther, D., Xu, J., Gao, C.G., Chen, H.H., 2008a. In situ analysis of major and trace elements of anhydrous minerals by LA–ICP–MS without applying an internal standard. Chemical Geology 257, 34–43.
Liu, Y.S., Hu, Z.C., Zong, K.Q., Gao, C.G., Gao, S., Xu, J., Chen, H.H., 2010b. Reappraisement and refinement of zircon U–Pb isotope and trace element analyses by LA–ICP–MS. Chinese Science Bulletin 55, 1535–1546.
Liu, Y.S., Yu, H.F., Xin, H.T., Lu, S.N., Xiu, Q.Y., Li, Q., 2009b. Tectonic units division and Precambrian significant geological events in Altyn Tagh Mountain, China. Geological Bulletin of China 28, 1430–1438.
Liu, Y.S., Zong, K.Q., Kelemen, P.B., Gao, S., 2008b. Geochemistry and magmatic history of eclogites and ultramafic rocks from the Chinese continental scientific drill hole: subduction and ultrahigh-pressure metamorphism of lower crustal cumulates. Chemical Geology 247, 133–153.
Long, X.P., Yuan, C., Sun, M., Xiao, W.J., Zhao, G.C., Zhou, K.F., Wang, Y.J., Hu, A.Q., 2011. The discovery of the oldest rocks in the Kuluketage area and its geological implications. Science in China (D) 54, 342–348.
Long, X.P., Yuan, C., Sun, M., Zhao, G.C., Xiao, W.J., Wang, Y.J., Yang, Y.H., Hu, A.Q., 2010. Archean crustal evolution of the northern Tarim craton, NW China: Zircon U–Pb and Hf isotopic constraints. Precambrian Research 180, 272–284.
Lu, S.N., Li, H.K., Zhang, C.L., Niu, G.H., 2008. Geological and geochronological evidence for the Precambrian evolution of the Tarim Craton and surrounding continental fragments. Precambrian Research 160, 94–107.
Ma, Q., Zheng, J.P., Griffin, W.L., Zhang, M., Tang, H.Y., Su, Y.P., Ping, X.Q., 2012. Triassic "adakitic" rocks in an extensional setting (North China): Melts from the cratonic lower crust. Lithos 149, 159–173.
Martin, H., 1999. Adakitic magmas: modern analogues of Archaean granitoids. Lithos 46, 411–429.
Martin, H., Smithies, R.H., Rapp, R., Moyen, J.F., Champion, D., 2005. An overview of adakite, tonalite–trondhjemite–granodiorite (TTG), and sanukitoid: relationships and some implications for crustal evolution. Lithos 79, 1–24.
Masuda, A., Nakamura, N., Tanaka, T., 1973. Fine structures of mutually normalized rare-earth patterns of chondrites. Geochimica et Cosmochimica Acta 37, 239–248.
McDonough, W.F., Sun, S.S., 1995. The composition of the Earth. Chemical Geology 120, 223–253.
Mei, H.L., Yu, H.F., Li, Q., 1997. Preliminary litho-tectonic framework of Early Precambrian rocks in Dunhuang-Beishan area, Guangsu, West China. Progress in Precambrian Research 20, 47–54 (in Chinese with English abstract).
Mei, H.L., Yu, H.F., Lu, S.N., Li, H.M., Lin, Y.X., Li, Q., 1998. Archean tonalite in the Dunhuang, Gansu province: age from the U–Pb single zircon and Nd isotope. Progress in Precambrian Research 21, 41–45 (in Chinese with English abstract).
Moyen, J.-F., Martin, H., 2012. Forty years of TTG research. Lithos 148, 312–336.
Nakajima, T., Maruyama, S., Uchiumi, S., Liou, J.G., Wang, X., Xiao, X., Graham, S.A., 1990. Evidence for late Proterozoic subduction from 700-Myr-old blueschists in China. Nature 346, 263–265.
Rapp, R.P., Shimizu, N., Norman, M.D., Applegate, G.S., 1999. Reaction between slab-derived melts and peridotite in the mantle wedge: experimental constraints at 3.8 GPa. Chemical Geology 160, 335–356.
Roberts, N.M.W., 2012. Increased loss of continental crust during supercontinent amalgamation. Gondwana Research 21, 994–1000.
Rubatto, D., 2002. Zircon trace element geochemistry: partitioning with garnet and the link between U–Pb ages and metamorphism. Chemical Geology 184, 123–138.
Rudnick, R.L., 1995. Making continental crust. Nature 378, 571–578.
Taylor, S.R., McLennan, S.M., 1995. The geochemical evolution of the continental crust. Reviews of Geophysics 33, 241–265.
Vervoort, J.D., Jonathan Patchett, P., 1996. Behavior of hafnium and neodymium isotopes in the crust: constraints from Precambrian crustally derived granites. Geochimica et Cosmochimica Acta 60, 3717–3733.
Wan, Y.S., Liu, D.Y., Wang, S.J., Yang, E.X., Wang, W., Dong, C.Y., Zhou, H.Y., Du, L.L., Yang, Y.H., Diwu, C.R., 2011. ~2.7 Ga juvenile crust formation in the North China Craton (Taishan-Xintai area, western Shandong Province): Further evidence of an understated event from U–Pb dating and Hf isotopic composition of zircon. Precambrian Research 186, 169–180.
Wu, F.Y., Zhang, Y.B., Yang, J.H., Xie, L.W., Yang, Y.H., 2008. Zircon U–Pb and Hf isotopic constraints on the Early Archean crustal evolution in Anshan of the North China Craton. Precambrian Research 167, 339–362.
Wu, M.L., Zhao, G.C., Sun, M., Li, S.Z., He, Y.H., Bao, Z.A., 2013. Zircon U–Pb geochronology and Hf isotopes of major lithologies from the Yishui Terrane: implications for the crustal evolution of the Eastern Block, North China Craton. Lithos 170–171, 164–178.
Wu, Y.B., Zheng, Y.F., Zhang, S.B., Zhao, Z.F., Wu, F.Y., Liu, X.M., 2007. Zircon U–Pb ages and Hf isotope compositions of migmatite from the North Dabie terrane in China: constraints on partial melting. Journal of Metamorphic Geology 25, 991–1009.
Yong, W.J., Zhang, L., Hall, C.M., Mukasa, S.B., Essene, E.J., 2013. The $^{40}Ar/^{39}Ar$ and Rb–Sr chronology of the Precambrian Aksu blueschists in western China. Journal of Asian Earth Sciences 63, 197–205.
Yu, H.F., Mei, H.L., Li, Q., 1998. The characteristics of Archean khondalite series in Dunhuang, Gansu Province. Progress in Precambrian Research 21, 19–25 (in Chinese with English abstract).
Zhang, C.L., Li, H.K., Santosh, M., Li, Z.X., Zou, H.B., Wang, H.Y., Ye, H.M., 2012a. Precambrian evolution and cratonization of the Tarim Block, NW China: Petrology, geochemistry, Nd-isotopes and U–Pb zircon geochronology from Archaean gabbro-TTG–potassic granite suite and Paleoproterozoic metamorphic belt. Journal of Asian Earth Sciences 47, 5–20.
Zhang, C.L., Zou, H.B., Li, H.K., Wang, H.Y., 2012b. Tectonic framework and evolution of the Tarim Block in NW China. Gondwana Research 23, 1306–1315.
Zhang, J., Gong, J., Yu, S., 2012c. 1.85 Ga HP granulite-facies metamorphism in the Dunhuang block of the Tarim Craton, NW China: evidence from U–Pb zircon dating of mafic granulites. Journal of the Geological Society 169, 511–514.
Zhang, J.X., Gong, J.H., Yu, S.Y., Li, H.K., Hou, K.J., 2013a. Neoarchean-Paleoproterozoic multiple tectonothermal events in the western Alxa block, North China Craton and their geological implication: Evidence from zircon U–Pb ages and Hf isotopic composition. Precambrian Research, http://dx.doi.org/10.1016/j.precamres.2013.05.002.
Zhang, J.X., Yu, S.Y., Gong, J.H., Li, H.K., Hou, K.J., 2013b. The latest Neoarchean–Paleoproterozoic evolution of the Dunhuang block, eastern Tarim craton, northwestern China: evidence from zircon U–Pb dating and Hf isotopic analyses. Precambrian Research 226, 21–42.
Zhang, S.B., Zheng, Y.F., Wu, Y.B., Zhao, Z.F., Gao, S., Wu, F.Y., 2006. Zircon isotope evidence for ≥3.5 Ga continental crust in the Yangtze craton of China. Precambrian Research 146, 16–34.
Zhao, G.C., Cawood, P.A., 2012. Precambrian geology of China. Precambrian Research 222–223, 13–54.
Zhao, G.C., Guo, J.H., 2012. Precambrian geology of China: preface. Precambrian Research 222–223, 1–12.

Zhao, G.C., Kroner, A., Wilde, S.A., Sun, M., Li, S.Z., Li, X.P., Zhang, J., Xia, X.P., He, Y.H., 2007. Lithotectonic elements and geological events in the Hengshan–Wutai–Fuping belt: a synthesis and implications for the evolution of the Trans-North China Orogen. Geological Magazine 144, 753–775.

Zhao, G.C., Zhai, M.G., 2013. Lithotectonic elements of Precambrian basement in the North China Craton: review and tectonic implications. Gondwana Research 23, 1207–1240.

Zheng, Y.F., Xiao, W.J., Zhao, G.C., 2013. Introduction to tectonics of China. Gondwana Research 23, 1189–1206.

Zong, K.Q., Liu, Y.S., Gao, C.G., Hu, Z.H., Gao, S., Gong, H.J., 2010. In situ U–Pb dating and trace element analysis of zircons in thin sections of eclogite: refining constraints on the UHP metamorphism of the Sulu terrane, China. Chemical Geology 269, 237–251.

Zong, K.Q., Zhang, Z.M., He, Z.Y., Hu, Z.C., Santosh, M., Liu, Y.S., Wang, W., 2012. Early Palaeozoic high-pressure granulites from the Dunhuang block, northeastern Tarim Craton: constraints on continental collision in the southern Central Asian Orogenic Belt. Journal of Metamorphic Geology 30, 753–768.